

Thermodynamic modes of a quasiperiodic mobility-edge system in a quantum Otto cycle

Ao Zhou,¹ Shujie Cheng,^{2, 1, *} and Gao Xianlong^{1, †}

¹*Department of Physics, Zhejiang Normal University, Jinhua 321004, China*

²*Xingzhi College, Zhejiang Normal University, Lanxi 321100, China*

(Dated: February 10, 2026)

We investigate thermodynamic operation of a quasiperiodic lattice with an exact mobility edge, described by the Biddle–Das Sarma model. We use this model as the working medium of a quantum Otto cycle and map its operating mode as a function of the hopping-range parameter p , the initial and final potential strengths V_i and V_f , and two idealized protocols for the isolated strokes. In a near-adiabatic (state-frozen) protocol, where the density matrix is approximately unchanged during the isolated strokes, the cycle supports only two modes: a *heater* and an *accelerator*. In an adiabatic protocol, where level populations are preserved while the spectrum is deformed, two additional modes appear: a *heat engine* and a *refrigerator*. Our results show that mobility-edge systems can realize multiple thermodynamic functions within a single platform and provide guidance for switching between modes by tuning p , V_i , and V_f .

I. INTRODUCTION

Quantum thermal devices were first placed on a clear footing by the proposal of a quantum heat engine based on a three-level maser¹. Since then, quantum heat engines and refrigerators have been studied extensively, both as models of energy conversion at small scales and as testbeds for nonequilibrium quantum thermodynamics^{2–28}. Many studies adapt familiar cycles—Carnot²⁹, Otto^{30,31}, Brayton^{32,33}, and Diesel³⁴—by replacing the classical working substance with a controllable quantum system. The cycle then converts heat and work according to quantum dynamics and thermalization³⁵.

A recurring theme is that the operating mode and performance can depend strongly on properties that have no classical counterpart, such as coherence⁶, dissipation mechanisms^{29,36}, interactions³⁷, and quantum critical points²⁴. This sensitivity suggests that systems with sharp spectral reorganizations may offer useful control knobs for switching between thermodynamic functions.

Quasiperiodic lattices provide a concrete setting where spectral and eigenstate properties can be tuned in a controlled way, and they have been explored as working media for quantum thermal cycles^{38–40}. In particular, recent work indicates that changes in eigenstate character (extended versus nonextended) can be correlated with changes in thermodynamic operating mode³⁹. For quasiperiodic models without mobility edges, a single Hamiltonian can support four modes (heat engine, refrigerator, heater, and accelerator) by tuning system parameters⁴⁰. By contrast, for quasiperiodic *mobility-edge* systems—where extended and localized states coexist at different energies—the thermodynamic landscape is less explored, and existing work has focused mainly on heat-engine operation³⁸. This motivates two practical questions: Which thermodynamic modes are accessible in a mobility-edge system, and under what conditions do they emerge?

In this paper we address these questions using the Biddle–Das Sarma model as a representative quasiperiodic mobility-edge system⁴¹. We embed the model in a quantum Otto cycle and construct mode diagrams as functions of the hopping-range parameter p and the potentials V_i and V_f , comparing a near-adiabatic (state-frozen) protocol and an adiabatic protocol for the isolated strokes. Section II summarizes the model and the mobility-edge condition, together with the localization measures used. Section III defines the Otto cycle, the heat and work conventions, and the two protocols for the isolated strokes. Section IV presents the resulting mode diagrams and discusses how mode competition depends on p , V_i , and V_f . Section V concludes with a summary and outlook.

II. BIDDLE–DAS SARMA MODEL

We consider the one-dimensional Biddle–Das Sarma model, introduced as a minimal quasiperiodic lattice with an exact mobility edge under exponentially decaying hopping⁴¹. The Hamiltonian reads

$$\hat{H} = \sum_{n,n' \neq n} t e^{-p|n-n'|} \left(\hat{c}_{n'}^\dagger \hat{c}_n + \hat{c}_n^\dagger \hat{c}_{n'} \right) + \sum_n V_n \hat{c}_n^\dagger \hat{c}_n, \quad (1)$$

where \hat{c}_n^\dagger (\hat{c}_n) creates (annihilates) a particle at site n , t sets the energy scale, and $p > 0$ controls how rapidly the hopping decays with distance. The onsite potential is quasiperiodic,

$$V_n = V \cos(2\pi\alpha n), \quad (2)$$

with irrational α (we use $\alpha = (\sqrt{5} - 1)/2$).

A defining property of the model is an analytic mobility edge obtained from self-duality⁴¹,

$$\frac{E_c}{t} = V \cosh(p) - 1, \quad (3)$$

which separates extended from localized single-particle eigenstates at energy E_c .

To characterize eigenstate localization numerically, we use the inverse participation ratio (IPR)⁴¹. For a normalized eigenstate $|\psi^{(j)}\rangle = \sum_{n=1}^L \phi_n^{(j)} \hat{c}_n^\dagger |0\rangle$, the IPR is

$$\text{IPR}^{(j)} = \sum_{n=1}^L \left| \phi_n^{(j)} \right|^4. \quad (4)$$

Extended states satisfy $\text{IPR} \sim 1/L$, while localized states yield $\text{IPR} = O(1)$ as L increases. We also report the associated fractal dimension

$$D^{(j)} = -\frac{\log \text{IPR}^{(j)}}{\log L}, \quad (5)$$

which approaches 1 for extended states and 0 for localized states in the large- L limit.

Figure 1 shows IPR and D across the spectrum as functions of V/t for two representative values of p . The mobility-edge line cleanly separates regions dominated by extended or localized eigenstates. A practical implication for the Otto-cycle setting is that changing p shifts the mobility edge: for smaller p the mobility edge occurs at larger V , while for larger p it moves to smaller V . In Sec. IV we show how this shift correlates with changes in the mode diagram of the Otto cycle.

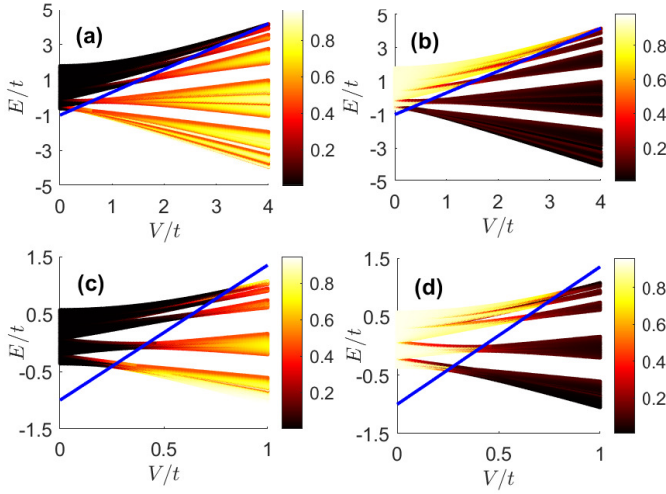


Figure 1. (Color online) (a) IPR at each energy level versus V/t for $p = 0.75$ and $L = 610$. (b) Fractal dimension D versus V/t for the same parameters. (c) IPR versus V/t for $p = 1.5$ and $L = 610$. (d) Fractal dimension D versus V/t for the same parameters. The color in (a) and (c) represent the IPR and that in (b) and (d) denote the fractal dimension D . The solid blue line denotes the mobility edge $E_c/t = V \cosh(p) - 1$.

III. QUANTUM OTTO CYCLE

We implement a four-stroke Otto cycle using the Biddle–Das Sarma model as the working medium. A

schematic is shown in Fig. 2. The control parameter is the onsite potential strength V , which is switched between V_i and V_f during the isolated strokes. The cycle consists of two thermalization strokes and two isolated strokes, in direct analogy with the classical Otto cycle^{42–45}.

During stroke ④ → ①, the system (with Hamiltonian $H(V_i)$) is coupled to a hot bath at temperature T_h and relaxes to thermal equilibrium. During stroke ② → ③, the system (with Hamiltonian $H(V_f)$) is coupled to a cold bath at temperature T_c and again equilibrates. Strokes ① → ② and ③ → ④ are carried out under thermal isolation, during which the Hamiltonian parameter is tuned from V_i to V_f and back. In practice, such isolated strokes need not be perfectly adiabatic because finite-time driving can induce transitions^{45,46}. Below we consider two limiting protocols that bracket possible behavior.

Let E_1, E_2, E_3, E_4 denote the internal energy at the four corners of the cycle. We define the heat absorbed from the hot bath, the heat released to the cold bath, and the net work output as

$$Q_h = E_1 - E_4, \quad Q_c = E_3 - E_2, \quad W = Q_h + Q_c. \quad (6)$$

With this convention, $W > 0$ corresponds to net work production. The cycle respects the Clausius inequality by construction. Following Refs. [45,46], we classify the operating mode by the signs of (Q_h, Q_c, W) :

1. *Heat engine*: $Q_h > 0, Q_c < 0, W > 0$;
2. *Refrigerator*: $Q_h < 0, Q_c > 0, W < 0$;
3. *Heater*: $Q_h < 0, Q_c < 0, W < 0$;
4. *Accelerator*: $Q_h > 0, Q_c < 0, W < 0$.

On the hot isochoric stroke, the density matrix is the Gibbs state

$$\rho_1 = \frac{e^{-\beta_h H(V_i)}}{Z_1}, \quad Z_1 = \text{Tr}[e^{-\beta_h H(V_i)}], \quad (7)$$

where $\beta_h = (k_B T_h)^{-1}$ and $E_1 = \text{Tr}[\rho_1 H(V_i)]$. On the cold isochoric stroke,

$$\rho_3 = \frac{e^{-\beta_c H(V_f)}}{Z_3}, \quad Z_3 = \text{Tr}[e^{-\beta_c H(V_f)}], \quad (8)$$

where $\beta_c = (k_B T_c)^{-1}$ and $E_3 = \text{Tr}[\rho_3 H(V_f)]$.

We now specify the two protocols for the isolated strokes.

Near-adiabatic (state-frozen) protocol. We assume that the density matrix changes negligibly during each isolated stroke, so the state is approximately “carried along” while the Hamiltonian parameter is switched. This limit can be interpreted as extremely fast switching or as active control that suppresses unwanted evolution, which can be approached using feedback techniques^{47–52}. We take $\rho_2 \simeq \rho_1$ and $\rho_4 \simeq \rho_3$, giving

$$E_2 = \text{Tr}[\rho_1 H(V_f)], \quad E_4 = \text{Tr}[\rho_3 H(V_i)]. \quad (9)$$

Adiabatic protocol. We assume that the isolated strokes are slow enough to preserve level populations in the instantaneous energy basis. Denote the single-particle energies of $H(V_i)$ and $H(V_f)$ by $\{E_j^i\}$ and $\{E_j^f\}$, respectively. Because the Hamiltonian is quadratic, equilibrium and mean energies can be evaluated from the single-particle spectrum. For convenience we use Fermi-Dirac occupations (equivalently, a grand-canonical description with chemical potential absorbed into the energy reference),

$$f_\beta(E) = (1 + e^{\beta E})^{-1}. \quad (10)$$

After thermalization with the hot bath, the occupations are $f_{\beta_h}(E_j^i)$; adiabatic evolution to V_f preserves these occupations while changing the energies, yielding

$$E_2 = \sum_{j=1}^L E_j^f f_{\beta_h}(E_j^i). \quad (11)$$

Similarly, after thermalization with the cold bath, the occupations are $f_{\beta_c}(E_j^f)$; adiabatic evolution back to V_i gives

$$E_4 = \sum_{j=1}^L E_j^i f_{\beta_c}(E_j^f). \quad (12)$$

These expressions reduce the cycle analysis to the spectra at V_i and V_f and provide a consistent basis for the mode diagrams in Sec. IV.

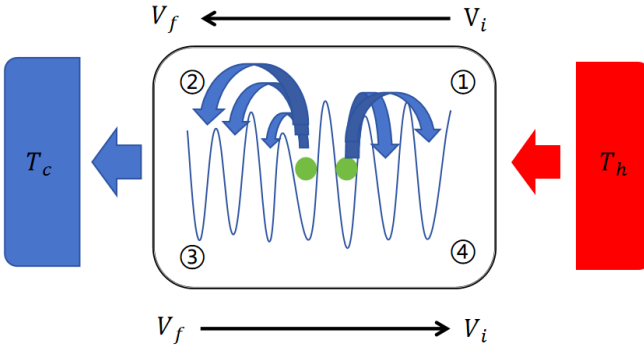


Figure 2. (Color online) Schematic of the quantum Otto cycle. Strokes ④ \rightarrow ① and ② \rightarrow ③ are thermalization at fixed Hamiltonians $H(V_i)$ and $H(V_f)$, with reservoirs at T_h and T_c . Strokes ① \rightarrow ② and ③ \rightarrow ④ are isolated parameter changes from V_i to V_f and back.

IV. MULTIPLE THERMODYNAMIC MODES

We now present the operating-mode diagrams obtained by evaluating Q_h , Q_c , and W over parameter space. We emphasize that the “mode” refers only to the sign structure of heat and work, as defined in Sec. III. We compare

the near-adiabatic (state-frozen) protocol and the adiabatic protocol, and we focus on how the hopping-range parameter p and the tuning amplitude V_f reshape the accessible regions.

A. Near-adiabatic (state-frozen) protocol

Figure 3 shows mode diagrams for $p = 0.75$ and $L = 233$ for several values of V_f . Only two modes appear: *heater* and *accelerator*. For small V_f [Figs. 3(a) and 3(b)], the accessible range of V_i is relatively narrow and the mode boundary is most sensitive to the hot-bath temperature T_h . In this regime, modest changes in T_h can switch the cycle between heater and accelerator operation. As V_f increases [Figs. 3(c) and 3(d)], the boundary shifts toward larger V_i , indicating that tuning V_i becomes an effective control knob at fixed T_h . The heater region initially expands with V_f but then approaches saturation: beyond a threshold, increasing V_f mainly enlarges accelerator-dominated regions. This behavior identifies a practical upper range of V_f for maximizing heater operation without unnecessary parameter excursions.

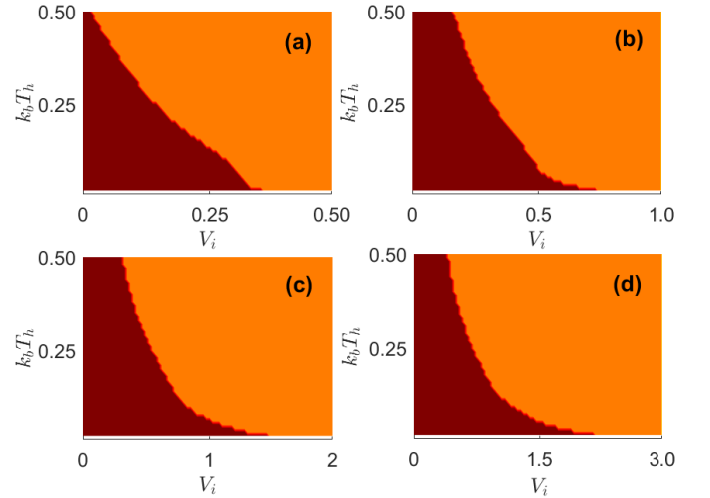


Figure 3. (Color online) Operating modes in the near-adiabatic (state-frozen) protocol for $p = 0.75$ and $L = 233$. (a) $V_f = 0.5t$; (b) $V_f = t$; (c) $V_f = 2t$; (d) $V_f = 3t$. Brown: *heater*. Yellow: *accelerator*.

Figure 4 shows the corresponding results for $p = 1.5$ and $L = 233$. The cycle again supports only heater and accelerator modes, but the heater region is more compressed and the boundary is more tilted in the (T_h, V_i) plane. This indicates increased sensitivity to *both* T_h and V_i : at fixed V_f , raising either parameter tends to favor the accelerator mode. As in the $p = 0.75$ case, the heater region grows with V_f and then saturates. Overall, increasing p reduces the parameter window in which heater operation is possible and lowers the corresponding T_h threshold. Within this protocol, the mobility-edge

structure therefore influences the *extent* and *sensitivity* of the heater region, even though no new modes appear.

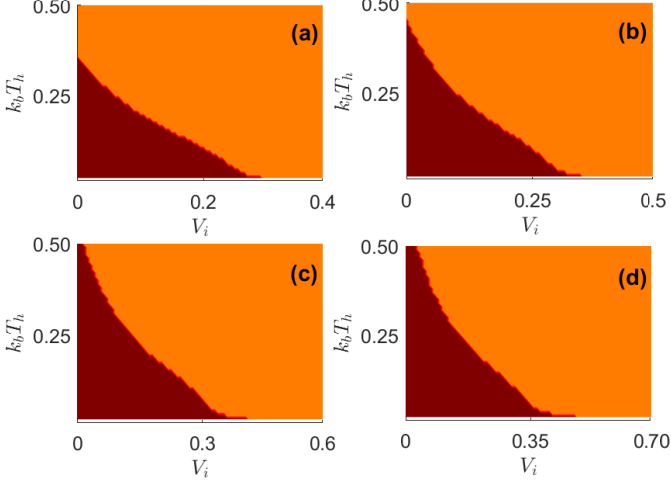


Figure 4. (Color online) Operating modes in the near-adiabatic (state-frozen) protocol for $p = 1.5$ and $L = 233$. (a) $V_f = 0.4t$; (b) $V_f = 0.5t$; (c) $V_f = 0.6t$; (d) $V_f = 0.7t$. Brown: *heater*. Yellow: *accelerator*.

B. Adiabatic protocol

We now turn to the adiabatic protocol, where the isolated strokes preserve level populations. In this case, the Otto cycle can access additional operating modes.

Figure 5 shows mode diagrams for $p = 0.75$ and $L = 610$ over a range of V_f values. For very small and very large V_f [Figs. 5(a) and 5(f)], the diagram resembles the near-adiabatic protocol, with only heater and accelerator modes. At intermediate V_f [Figs. 5(b)–5(d)], two additional modes emerge at low T_h : a *heat engine* and a *refrigerator*. In this regime, mode boundaries become densely packed, and varying V_i at fixed (T_h, V_f) can switch the cycle among three or more modes. The refrigerator region is the most constrained, requiring both low T_h and a narrow range of (V_i, V_f) . As V_f increases further [Figs. 5(d)–5(f)], the refrigerator region disappears first, while the heat-engine region shrinks more gradually. The heat-engine region also competes directly with the heater region: when the heat-engine window grows, the heater window is compressed, and vice versa.

Figure 6 shows the same analysis for $p = 1.5$ and $L = 610$. The high- T_h region is again dominated by accelerator operation, while the low- T_h region supports heater, heat-engine, and refrigerator modes over intermediate V_f . Compared with $p = 0.75$, the heat-engine window is more structured: it appears most prominently when V_i and V_f are close and can split as V_f increases. This splitting is accompanied by a narrowing of the allowable T_h range, indicating stronger parameter constraints for stable heat-engine operation. In contrast, the refriger-

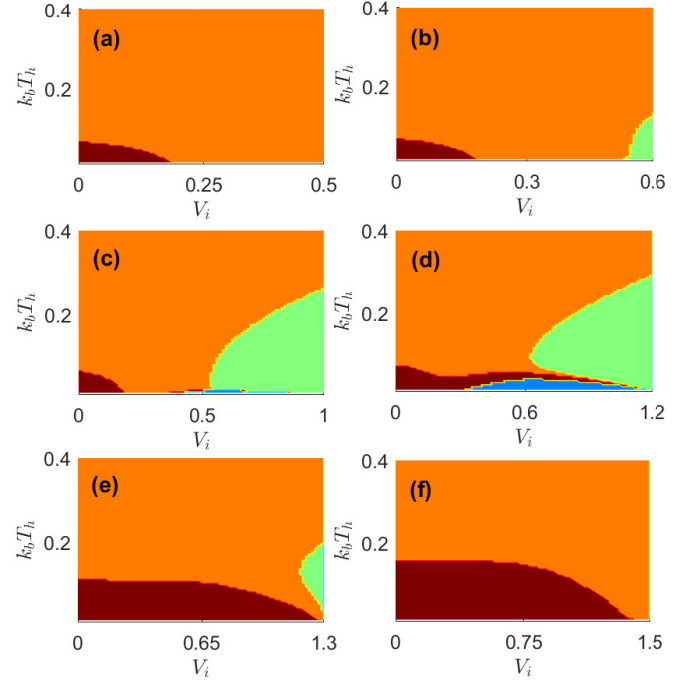


Figure 5. (Color online) Operating modes in the adiabatic protocol for $p = 0.75$ and $L = 610$. (a) $V_f = 0.5t$; (b) $V_f = 0.6t$; (c) $V_f = t$; (d) $V_f = 1.2t$; (e) $V_f = 1.3t$; (f) $V_f = 1.5t$. Brown: *heater*. Yellow: *accelerator*. Green: *heat engine*. Blue: *refrigerator*.

erator window can remain visible over a wider span of V_f in the large- p case, suggesting improved robustness of refrigerator operation relative to heat-engine operation in this parameter regime. As V_f increases, the heat-engine area typically contracts before the refrigerator area does, and the heater region can expand back toward a saturated extent once the competing modes diminish.

Taken together, Figs. 5 and 6 show that the adiabatic protocol unlocks the full set of four thermodynamic modes, but only within parameter windows that depend on both the spectrum deformation (set by V_f) and the hopping range (set by p). In particular, moderate V_f is essential: too small or too large a change tends to suppress the heat-engine and refrigerator windows, returning the cycle to the simpler two-mode behavior.

V. SUMMARY

We studied thermodynamic operation of a quasiperiodic mobility-edge lattice, described by the Biddle-Das Sarma model⁴¹, when used as the working medium of a quantum Otto cycle. We mapped the operating mode as a function of the hopping-range parameter p , the initial and final onsite potentials V_i and V_f , and the protocol used for the isolated strokes.

In a near-adiabatic (state-frozen) protocol, the cycle

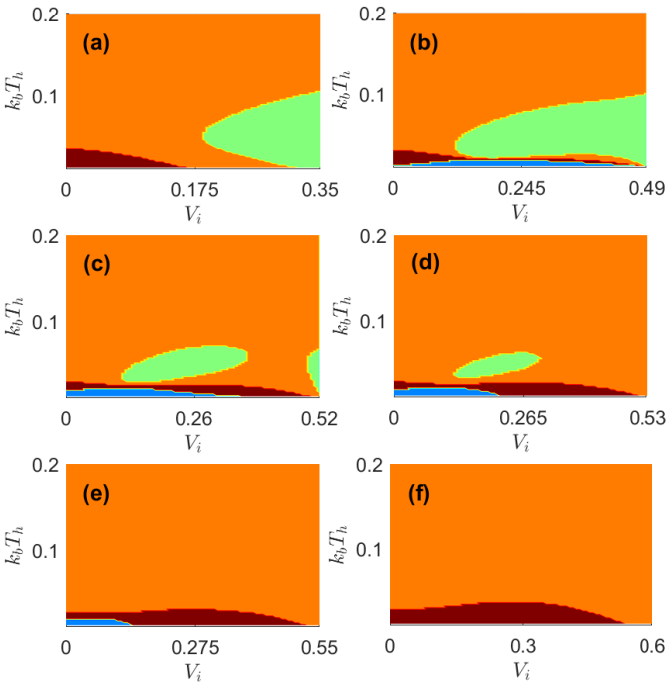


Figure 6. (Color online) Operating modes in the adiabatic protocol for $p = 1.5$ and $L = 610$. (a) $V_f = 0.35t$; (b) $V_f = 0.49t$; (c) $V_f = 0.52t$; (d) $V_f = 0.53t$; (e) $V_f = 0.55t$; (f) $V_f = 0.6t$. Brown: heater. Yellow: accelerator. Green: heat engine. Blue: refrigerator.

supports only two modes, heater and accelerator, with mode boundaries that shift systematically as V_f is increased and that show clear saturation behavior. In an adiabatic protocol, the cycle exhibits four modes: heater, accelerator, heat engine, and refrigerator. The heat-engine and refrigerator windows appear mainly at low T_h and intermediate V_f , where competition among modes is strongest. We further find that increasing p reshapes these windows: the heat-engine region can become more constrained and fragmented, while the refrigerator region can remain comparatively robust in the parameter ranges studied.

Our results highlight that mobility-edge systems can serve as tunable, multifunctional working media for quantum thermal cycles. An important next step is to broaden the operating windows of the heat-engine and refrigerator modes, for example by refining the cycle protocol beyond the two limiting cases considered here. Such extensions would help assess how robust these mode diagrams remain under more realistic finite-time driving and experimental constraints.

ACKNOWLEDGMENTS

This research is supported by Zhejiang Provincial Natural Science Foundation of China under Grant No. LQN25A040012, the National Natural Science Foundation of China under Grant No. 12174346, and the start-up fund from Xingzhi College, Zhejiang Normal University.

* chengsj@zjnu.edu.cn

† gaoxl@zjnu.edu.cn

¹ H. E. D. Scovil and E. O. Schulz-DuBois, “Three-Level Masers as Heat Engines,” *Physical Review Letters* **2**, 262–263 (1959).

² T. D. Kieu, “Quantum heat engines, the second law and Maxwell’s daemon,” *The European Physical Journal D* **39**, 115–128 (2006).

³ Ji-Zhou He, Xian He, and Jie Zheng, “Thermal Entangled Quantum Heat Engine Working with a Three-Qubit Heisenberg XX Model,” *International Journal of Theoretical Physics* **51**, 2066–2076 (2012).

⁴ H. T. Quan, Yu-xi Liu, C. P. Sun, and Franco Nori, “Quantum thermodynamic cycles and quantum heat engines,” *Physical Review E* **76**, 031105 (2007).

⁵ Ting Zhang, Wei-Tao Liu, Ping-Xing Chen, and Cheng-Zu Li, “Four-level entangled quantum heat engines,” *Physical Review A* **75**, 062102 (2007).

⁶ Marlan O. Scully, M. Suhail Zubairy, Girish S. Agarwal, and Herbert Walther, “Extracting Work from a Single Heat Bath via Vanishing Quantum Coherence,” *Science* **299**, 862–864 (2003).

⁷ G. F. Zhang, “Entangled quantum heat engines based on two two-spin systems with Dzyaloshinskii-Moriya anisotropic antisymmetric interaction,” *The European*

Physical Journal D **49**, 123 (2008).

⁸ Markus J. Henrich, Günter Mahler, and Mathias Michel, “Driven spin systems as quantum thermodynamic machines: Fundamental limits,” *Physical Review E* **75**, 051118 (2007).

⁹ X L Huang, Huan Xu, X Y Niu, and Y D Fu, “A special entangled quantum heat engine based on the two-qubit Heisenberg XX model,” *Physica Scripta* **88**, 065008 (2013).

¹⁰ Hao Wang, Guoxing Wu, and Daojiong Chen, “Thermal entangled quantum Otto engine based on the two qubits Heisenberg model with Dzyaloshinskii–Moriya interaction in an external magnetic field,” *Physica Scripta* **86**, 015001 (2012).

¹¹ Hao Wang, Sanqiu Liu, and Jizhou He, “Thermal entanglement in two-atom cavity QED and the entangled quantum Otto engine,” *Physical Review E* **79**, 041113 (2009).

¹² Andrea Solfanelli, Guido Giachetti, Michele Campisi, Stefano Ruffo, and Nicolò Defenu, “Quantum heat engine with long-range advantages,” *New Journal of Physics* **25**, 033030 (2023).

¹³ R. Shankar and Ganpathy Murthy, “Nearest-neighbor frustrated random-bond model in $d=2$: Some exact results,” *Physical Review B* **36**, 536–545 (1987).

¹⁴ George Thomas and Ramandeep S. Johal, “Coupled quan-

tum Otto cycle,” *Physical Review E* **83**, 031135 (2011).

¹⁵ Ferdi Altintas and Özgür E. Müstecaplıoğlu, “General formalism of local thermodynamics with an example: Quantum Otto engine with a spin- 1 / 2 coupled to an arbitrary spin,” *Physical Review E* **92**, 022142 (2015).

¹⁶ Tova Feldmann and Ronnie Kosloff, “Quantum four-stroke heat engine: Thermodynamic observables in a model with intrinsic friction,” *Physical Review E* **68**, 016101 (2003).

¹⁷ E. A. Ivanchenko, “Quantum Otto cycle efficiency on coupled qudits,” *Physical Review E* **92**, 032124 (2015).

¹⁸ M. Azimi, L. Chotorlishvili, S. K. Mishra, T. Vekua, W. Hübner, and J. Berakdar, “Quantum Otto heat engine based on a multiferroic chain working substance,” *New Journal of Physics* **16**, 063018 (2014).

¹⁹ W. Hübner, G. Lefkidis, C. D. Dong, D. Chaudhuri, L. Chotorlishvili, and J. Berakdar, “Spin-dependent Otto quantum heat engine based on a molecular substance,” *Physical Review B* **90**, 024401 (2014).

²⁰ Nikos K. Kollas and Dimitris Moustos, “An exactly solvable relativistic quantum Otto engine,” *Physical Review D* **109**, 065025 (2024), 2312.06452 [quant-ph].

²¹ Jin-Fu Chen, Chang-Pu Sun, and Hui Dong, “Boosting the performance of quantum Otto heat engines,” *Physical Review E* **100**, 032144 (2019).

²² Selçuk Çakmak, Ferdi Altintas, and Özgür E. Müstecaplıoğlu, “Lipkin-Meshkov-Glick Model in a Quantum Otto Cycle,” *The European Physical Journal Plus* **131**, 197 (2016), 1510.04495 [quant-ph].

²³ Bruno Leggio and Mauro Antezza, “Otto engine beyond its standard quantum limit,” *Physical Review E* **93**, 022122 (2016).

²⁴ Aslı Tuncer and Batu Yalçın, “Quantum Ising Spin-Glass Otto Engine,” (2024), 2405.03495 [quant-ph].

²⁵ Jianhui Wang, Zhaoqi Wu, and Jizhou He, “Quantum Otto engine of a two-level atom with single-mode fields,” *Physical Review E* **85**, 041148 (2012).

²⁶ Giulia Piccitto, Michele Campisi, and Davide Rossini, “The Ising critical quantum Otto engine,” *New Journal of Physics* **24**, 103023 (2022).

²⁷ A. Rodin, “Three-dimensional harmonic oscillator as a quantum Otto engine,” *Physical Review Research* **6**, 013180 (2024).

²⁸ Mark T. Mitchison, “Quantum thermal absorption machines: Refrigerators, engines and clocks,” *Contemporary Physics* **60**, 164–187 (2019).

²⁹ H. T. Quan, P. Zhang, and C. P. Sun, “Quantum-classical transition of photon-Carnot engine induced by quantum decoherence,” *Physical Review E* **73**, 036122 (2006).

³⁰ He-Guang Xu, Jiasen Jin, G. D. M. Neto, and Norton G. De Almeida, “Universal quantum Otto heat machine based on the Dicke model,” *Physical Review E* **109**, 014122 (2024).

³¹ Suman Chand, Shubhrangshu Dasgupta, and Asoka Biswas, “Finite-time performance of a single-ion quantum Otto engine,” *Physical Review E* **103**, 032144 (2021).

³² Feng Wu, Lingen Chen, Fengrui Sun, Chih Wu, and Qing Li, “Generalized model and optimum performance of an irreversible quantum Brayton engine with spin systems,” *Physical Review E* **73**, 016103 (2006).

³³ X. L. Huang, L. C. Wang, and X. X. Yi, “Quantum Brayton cycle with coupled systems as working substance,” *Physical Review E* **87**, 012144 (2013).

³⁴ C. D. Dong, G. Lefkidis, and W. Hübner, “Magnetic quantum diesel engine in n_2 ,” *Phys. Rev. B* **88**, 214421 (2013).

³⁵ Ronnie Kosloff, “Quantum Thermodynamics: A Dynamical Viewpoint,” *Entropy* **15**, 2100–2128 (2013).

³⁶ Ali Ü. C. Hardal and Özgür E. Müstecaplıoğlu, “Superradiant Quantum Heat Engine,” *Scientific Reports* **5**, 12953 (2015).

³⁷ G. F. Zhang, “Entangled quantum heat engines based on two two-spin systems with Dzyaloshinski-Moriya anisotropic antisymmetric interaction,” *The European Physical Journal D* **49**, 123 (2008).

³⁸ Cecilia Chiaracane, Mark T. Mitchison, Archak Purkayastha, Géraldine Haack, and John Goold, “Quasiperiodic quantum heat engines with a mobility edge,” *Physical Review Research* **2**, 013093 (2020).

³⁹ He-Guang Xu and Shujie Cheng, “Quantum transport property and thermodynamic applications of one-dimensional off-diagonal quasiperiodic system,” *Physical Review B* **112**, 24204 (2025), arXiv:2410.17550 [cond-mat].

⁴⁰ Shan Suo, Ao Zhou, Yanting Chen, Shujie Cheng, and Gao Xianlong, “Wigner distribution, wigner entropy and quantum refrigerator of a one-dimensional off-diagonal quasicrystal,” (2026), arXiv:2601.17691 [cond-mat].

⁴¹ J. Biddle and S. Das Sarma, “Predicted mobility edges in one-dimensional incommensurate optical lattices: An exactly solvable model of anderson localization,” *Phys. Rev. Lett.* **104**, 070601 (2010).

⁴² J. Deng, Q.-H. Wang, Z. Liu, P. Hänggi, and J. Gong, “Quantum Otto engines with finite-time discontinuities,” *Phys. Rev. E* **88**, 062122 (2013).

⁴³ Y. Zheng, P. Hänggi, and D. Poletti, “Occurrence of discontinuities in the performance of finite-time quantum Otto cycles,” *Phys. Rev. E* **94**, 012137 (2016).

⁴⁴ R. Kosloff and Y. Rezek, “The quantum harmonic Otto cycle,” *Entropy* **19**, 136 (2017).

⁴⁵ A. Solfanelli, M. Falsetti, and M. Campisi, “Nonadiabatic single-qubit quantum Otto engine,” *Phys. Rev. B* **101**, 054513 (2020).

⁴⁶ L. Buffoni, A. Solfanelli, P. Verrucchi, A. Cuccoli, and M. Campisi, “Quantum measurement cooling,” *Phys. Rev. Lett.* **122**, 070603 (2019).

⁴⁷ Clément Sayrin, Igor Dotsenko, Xingxing Zhou, Bruno Peaudecerf, Théo Rybarczyk, Sébastien Gleyzes, Pierre Rouchon, Mazyar Mirrahimi, Hadis Amini, Michel Brune, Jean-Michel Raimond, and Serge Haroche, “Real-time quantum feedback prepares and stabilizes photon number states,” *Nature* **477**, 73–77 (2011).

⁴⁸ R. Vijay, C. Macklin, D. H. Slichter, S. J. Weber, K. W. Murch, R. Naik, A. N. Korotkov, and I. Siddiqi, “Stabilizing Rabi oscillations in a superconducting qubit using quantum feedback,” *Nature* **490**, 77–80 (2012).

⁴⁹ Jordan M. Horowitz and Kurt Jacobs, “Quantum effects improve the energy efficiency of feedback control,” *Physical Review E* **89**, 42134 (2014).

⁵⁰ Jing Zhang, Yu-xi Liu, Re-Bing Wu, Kurt Jacobs, and Franco Nori, “Quantum feedback: Theory, experiments, and applications,” *Physics Reports* **679**, 1–60 (2017).

⁵¹ H. Uys, H. Bassa, P. Du Toit, S. Ghosh, and T. Konrad, “Quantum control through measurement feedback,” *Physical Review A* **97**, 60102 (2018).

⁵² Kacper Prech, Joël Aschwanden, and Patrick P. Potts, “Quantum thermodynamics of continuous feedback control,” (2025), arXiv:2505.16615 [quant-ph].